AIAA JOURNAL
Vol. 38, No. 5, May 2000

Enhanced Aeroelastic Analysis of Panels Under Transitory Hypersonic Flow Conditions

Radu Udrescu*
Comoti, S.A., 76194 Bucharest, Romania
and
Giuseppe Surace†
Politecnico di Torino, 10129 Turin, Italy

Computational analysis of transient hypersonic flow effects on high-speed or reentry space vehicles with panel substructures demonstrates the complexity of the aerothermoelastic behavior. Under certain transitory flow conditions (depending on the rate of change in dynamic pressures and thermal loads), the dynamic response rapidly changes its pattern when crossing the stable/unstable domains of the stability map. An interesting investigation of the dynamics of chaos of a deterministic system is offered. Apparently, the dynamic pattern should be related to the classical map of the aeroelastic stability boundaries, but the numerical solutions do not always confirm this assumption. The sensitivity of the nonlinear aerothermoelastic model to initial conditions that is characteristic of chaotic systems could explain this complex behavior.

Nomenclature

$\boldsymbol{A}$	= aerodynamic stiffness matrix
a, h	= panel length and thickness
$\boldsymbol{B}$	= aerodynamic damping matrix
c	= speed of sound
D	= plate rigidity
$\boldsymbol{K}$	= elastic stiffness matrix
$\boldsymbol{M}$	= mass matrix
M_∞	= Mach number
m	= mass per square meter
N	= normal tension
q_∞	= dynamic pressure
$\boldsymbol{r}$	= vector of degrees of freedom
U	= flow velocity
u, v, w	= displacements
x, y, z	= Cartesian coordinates
α	= coefficient of thermal expansion
$\Delta p_a, \Delta p_s$	= pressure (aerodynamic, static)
ΔT	= temperature change
δ	= damping parameter
ε	= strain
λ^r	= nondimensional dynamic pressure
ν	= Poisson's ratio
ρ_∞	= air density
σ	= stress
σ_x	= nondimensional buckling load
τ	= nondimensional time parameter

Subscripts

b	= bending
m	= membrane

Superscripts

t	= transpose
0	= nondimensional

Presented as Paper 99-1432 at the AIAA/ASME/ASCE/AHS/ASC 40th Structures, Structural Dynamics, and Materials Conference, St. Louis, MO, 12–15 April 1999; received 11 June 1999; revision received 13 September 1999; accepted for publication 13 September 1999.

*Research Scientist, P.O. Box 76/174, National Institute for Research and Development of Turbomachinery, Bd. Iuliu Maniu 220. Senior Member AIAA.
†Professor, Department of Aeronautical and Space Engineering, Corso Duca degli Abruzzi 24.

Introduction

CHAOTIC oscillations have been observed in nonlinear mechanical systems by using analytical, numerical, and experimental methods. A partial list[1] includes the following: vibrations of buckled elastic structures, mechanical systems with play or backlash, nonlinear aeroelastic systems, wheel–rail dynamics in rail systems, large three-dimensional vibrations of beams and shells, and systems with sliding friction. The fluttering buckled panels subjected to high-speed airflow (Fig. 1) give an interesting application of the dynamics of chaos in aircraft structures.

Within the classical approach,[2–4] the governing partial differential equation is reduced to a system of ordinary differential equations by using modal expansion and Galerkin's method. The finite elements method (FEM) has provided new capabilities for complex panel configurations. Olson[5] and Han and Yang[6] extended the FEM for linear and nonlinear three-dimensional isotropic plates, respectively. In addition, Xue and Mei[7] also considered the effect of arbitrary steady temperature. In Refs. 8 and 9 studies of nonlinear flutter of composite panels were conducted; in Refs. 10–12 the piezoelectric actuation method was successfully applied to control and suppress the flutter phenomenon.

No significant study has been directed toward failure mechanisms. However, at least two mechanisms are readily identifiable and have occurred in practice: 1) If the stress amplitude due to flutter exceeds the yield stress of the plate material over a substantial portion of the structure, then catastrophic or rapid failure occurs. 2) If the stresses are relatively small, then fatigue or long-time failure may occur. Recent studies[13,14] reported the fatigue analysis of two- and three-dimensional nonlinear panel models subjected to steady supersonic flow conditions.

All of the mentioned studies dealt with constant high-speed flow conditions (in terms of dynamic pressure and/or thermal buckling loads). The purpose of this paper is to extend the analysis by taking into account a more realistic model of the phenomenon, consisting of transitory changes of both parameters, assumed as having increasing values until stagnation levels are reached. The high-order finite element model proposed by the authors has already proved its virtues in investigating the aeroelasticity of panels by solving the classical problem[15] and in its extension to the transitory phenomena of supersonic field flow.[16]

Governing Equations

The von Kármán nonlinear strain-displacement relations for a general isotropic Hookean plate element undergoing both extension and bending at any point z are a sum of membrane and change of curvature strain components:

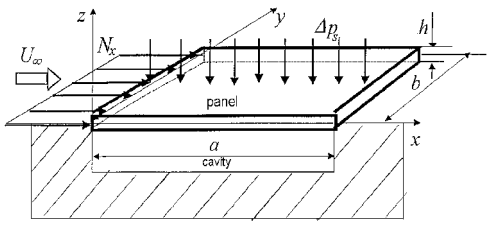

Fig. 1 Skew of the three-dimensional panel configuration.

$$\varepsilon_{xx} = \frac{\partial u}{\partial x} + \frac{1}{2}\left(\frac{\partial w}{\partial x}\right)^2 - z\frac{\partial^2 w}{\partial x^2} = \varepsilon_{xx0} - z\frac{\partial^2 w}{\partial x^2}$$

$$\varepsilon_{yy} = \frac{\partial v}{\partial y} + \frac{1}{2}\left(\frac{\partial w}{\partial y}\right)^2 - z\frac{\partial^2 w}{\partial y^2} = \varepsilon_{yy0} - z\frac{\partial^2 w}{\partial y^2}$$

$$\varepsilon_{xy} = \frac{\partial v}{\partial x} + \frac{\partial u}{\partial y} + \frac{\partial w}{\partial x}\frac{\partial w}{\partial y} - 2z\frac{\partial^2 w}{\partial x\,\partial y} = \varepsilon_{xy0} - 2z\frac{\partial^2 w}{\partial x\,\partial y} \quad (1)$$

If the plate is subjected to an uniform temperature difference ΔT, the stresses state can be written as the sum of the tension created by the stretching of the plate due to bending and the thermal applied in-plane load:

$$\sigma_{xx} = [E/(1-\nu^2)][\varepsilon_{yy} + \nu\varepsilon_{xx}] - [E/(1-\nu)]\alpha\Delta T$$

$$\sigma_{yy} = [E/(1-\nu^2)][\varepsilon_{xx} + \nu\varepsilon_{yy}] - [E/(1-\nu)]\alpha\Delta T$$

$$\sigma_{xy} = [E/2(1+\nu)]\varepsilon_{xy} \quad (2)$$

The tensions N_x, N_y, and N_{xy} defined by the relations

$$N_x = \int_{-h/2}^{h/2}\sigma_{xx}\,\mathrm{d}z, \qquad N_y = \int_{-h/2}^{h/2}\sigma_{yy}\,\mathrm{d}z, \qquad N_{xy} = \int_{-h/2}^{h/2}\sigma_{xy}\,\mathrm{d}z \quad (3)$$

are used in expressing the stretching and pure bending energy components

$$U_S = \frac{1}{2}\iint [N_x\varepsilon_{xx0} + N_y\varepsilon_{yy0} + N_{xy}\varepsilon_{xy0}]\,\mathrm{d}x\,\mathrm{d}y$$

$$U_B = \frac{D}{2}\iint\left[\left(\frac{\partial^2 w}{\partial x^2}\right)^2 + \left(\frac{\partial^2 w}{\partial y^2}\right)^2\right]\mathrm{d}x\,\mathrm{d}y$$

$$+ \frac{D}{2}\iint\left[2\nu\frac{\partial^2 w}{\partial x^2}\frac{\partial^2 w}{\partial y^2} + 2(1-\nu)\left(\frac{\partial^2 w}{\partial x\,\partial y}\right)^2\right]\mathrm{d}x\,\mathrm{d}y \quad (4)$$

The governing equation is obtained through the application of Hamilton's principle,

$$\int(\delta T - \delta U + \delta W)\,\mathrm{d}t = 0 \quad (5)$$

and has the known expression

$$D\Delta^2 w - N_x\frac{\partial^2 w}{\partial x^2} - N_y\frac{\partial^2 w}{\partial y^2} + m\frac{\partial^2 w}{\partial t^2} + \Delta p_a = \Delta p_s \quad (6)$$

where Δp_s is the transversal static aerodynamic pressure. For the aerodynamic terms, the simplest approximation valid for the domain of high-speed velocities is given by the first-order piston theory:

$$\Delta p_a = \frac{2q_\infty}{M_\infty^2}\left(\frac{\partial w}{\partial x} + \frac{1}{v_\infty}\frac{\partial w}{\partial t}\right) \quad (7)$$

This popular aerodynamic approximation predicts accurately the flow phenomenon at high Mach numbers. Moreover, Bailie and McFeely[17] have shown that their results in panel flutter analysis obtained using a full unsteady hypersonic theory agree very closely with the results of this approximate theory.

Finite Element Formulation

The finite element idealization is based on the elastic theory of the strains and stresses along the natural directions of a triangular finite element. Mainly, the modeling procedure consists of the Argyris high-order triangular finite elements[18] (fully compatible elements for the out-of-plane and in-plane displacements, respectively, based on the natural geometry concept). Two nets of identical topology and material properties create the finite elements model: 1) One is composed of fifth-order (six nodes) triangular plate elements. The 21 degrees of freedom of this element consist of displacement, all first and second derivatives at the vertices, for satisfying the continuity condition in curvature, and the normal derivative in the middle-points of the edges. 2) The other is composed of a second-order triangular membrane elements with 12 degrees of freedom per element, having no flexural stiffness and carrying loads by axial and central shear forces.

Thus, the finite element formulation of the general aerothermoelastic Eq. (6) can be written (in a nondimensional form) by using separate matrix components of plate and membrane terms

$$\begin{bmatrix} \boldsymbol{M}^0_{bb} & \boldsymbol{0} \\ \boldsymbol{0}^t & \boldsymbol{M}^0_{mm} \end{bmatrix}\begin{bmatrix} \ddot{\boldsymbol{r}}^0_b \\ \ddot{\boldsymbol{r}}^0_m \end{bmatrix} + \sqrt{\frac{\delta\lambda^r}{M_\infty}}\begin{bmatrix} \boldsymbol{B}^0 & \boldsymbol{0} \\ \boldsymbol{0}^t & \boldsymbol{0} \end{bmatrix}\begin{bmatrix} \dot{\boldsymbol{r}}^0_b \\ \dot{\boldsymbol{r}}^0_m \end{bmatrix}$$

$$+ \left(\lambda^r\begin{bmatrix} \boldsymbol{A}^0 & \boldsymbol{0} \\ \boldsymbol{0}^t & \boldsymbol{0} \end{bmatrix} + \begin{bmatrix} \boldsymbol{K}^0_{bb} + \sigma_x\boldsymbol{K}^0_g & \boldsymbol{0} \\ \boldsymbol{0}^t & \boldsymbol{K}^0_{mm} \end{bmatrix} + \begin{bmatrix} \boldsymbol{K}^0_{1bb} & \boldsymbol{K}^0_{1bm} \\ \boldsymbol{K}^0_{1mb} & \boldsymbol{0} \end{bmatrix}\right.$$

$$\left. + \begin{bmatrix} \boldsymbol{K}^0_{2bb} & \boldsymbol{0} \\ \boldsymbol{0}^t & \boldsymbol{0} \end{bmatrix}\right)\begin{bmatrix} \boldsymbol{r}^0_b \\ \boldsymbol{r}^0_m \end{bmatrix} = \begin{bmatrix} p_r\boldsymbol{P}^0_s \\ \sigma_x\boldsymbol{P}^0_x \end{bmatrix} \quad (8)$$

where $\boldsymbol{M}$, $\boldsymbol{B}$, $\boldsymbol{A}$, and $\boldsymbol{K}$ are the global mass, aerodynamic damping, influence, and linear elastic stiffness matrices, respectively; $\boldsymbol{K}_g$ is the geometric stiffness due to thermal forces; $\boldsymbol{K}_1$ and $\boldsymbol{K}_2$ are the nonlinear elastic stiffness matrices that depend linearly and quadratically on element plate $\boldsymbol{r}_b$ and membrane $\boldsymbol{r}_m$ displacements, respectively; $\boldsymbol{P}_s$ and $\boldsymbol{P}_x$ are the externally applied out-of-plane (static pressure) and in-plane loads. Dowell's nondimensional parameters

$$\zeta = t\sqrt{D/ma^4}, \qquad W = w/h, \qquad \delta = \rho_\infty a/m$$

$$\sigma_x = N_{x0}a^2/D, \qquad \lambda^r = \rho_\infty U_\infty^2 a^3/M_\infty D$$

$$p_r = \Delta p_s a^4/Dh \quad (9)$$

have the advantage of expressing the various results most compactly.

In the classical approach, the aerothermoelastic system Eq. (8) has been modeled as a differential equations system with constant terms. The solution is a sum of a time-dependent homogeneous solution (having the physical meaning of self-excited dynamic oscillations) and a time-independent particular solution (having the physical meaning of a thermal-aerodynamic static equilibrium deflection):

$$\boldsymbol{r} = \boldsymbol{r}_s + \boldsymbol{r}_t(t) \quad (10)$$

Xue and Mei[7] studied this aeroelastic model by separating Eq. (8) in two parts: a set of nonlinear algebraic equations that yields the thermal aerodynamic deflection

$$\left(\lambda^r\begin{bmatrix} \boldsymbol{A}^0 & \boldsymbol{0} \\ \boldsymbol{0}^t & \boldsymbol{0} \end{bmatrix} + \begin{bmatrix} \boldsymbol{K}^0_{bb} + \sigma_x\boldsymbol{K}^0_g & \boldsymbol{0} \\ \boldsymbol{0}^t & \boldsymbol{K}^0_{mm} \end{bmatrix}\right)\begin{bmatrix} \boldsymbol{r}^0_b \\ \boldsymbol{r}^0_m \end{bmatrix}_s$$

$$+ \left(\begin{bmatrix} \boldsymbol{K}^0_{1bb} & \boldsymbol{K}^0_{1bm} \\ \boldsymbol{K}^0_{1mb} & \boldsymbol{0} \end{bmatrix}_s + \begin{bmatrix} \boldsymbol{K}^0_{2bb} & \boldsymbol{0} \\ \boldsymbol{0}^t & \boldsymbol{0} \end{bmatrix}_s\right)\begin{bmatrix} \boldsymbol{r}^0_b \\ \boldsymbol{r}^0_m \end{bmatrix}_s = \begin{bmatrix} p_r\boldsymbol{P}^0_s \\ \sigma_x\boldsymbol{P}^0_x \end{bmatrix} \quad (11)$$

and a set of nonlinear differential homogeneous (self-excited) equations that yields the limit cycle motion

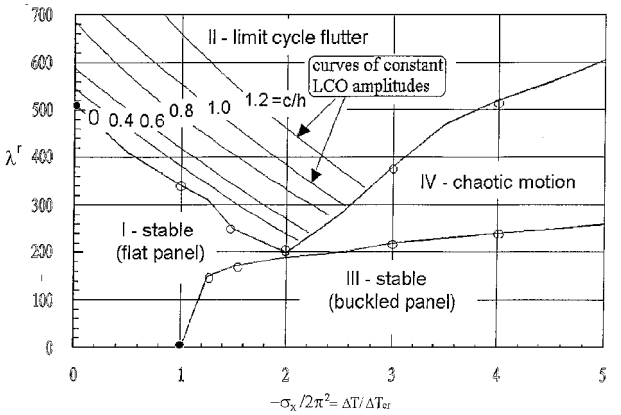

Fig. 2 Map of the aerothermoelastic stability boundary.

$$\begin{bmatrix} \boldsymbol{M}^0_{bb} & \boldsymbol{0} \\ \boldsymbol{0}^t & \boldsymbol{M}^0_{mm} \end{bmatrix} \begin{bmatrix} \ddot{\boldsymbol{r}}^0_b \\ \ddot{\boldsymbol{r}}^0_m \end{bmatrix}_t + \sqrt{\frac{\lambda^r}{M_\infty}} \begin{bmatrix} \boldsymbol{B}^0 & \boldsymbol{0} \\ \boldsymbol{0}^t & \boldsymbol{0} \end{bmatrix} \begin{bmatrix} \dot{\boldsymbol{r}}^0_b \\ \dot{\boldsymbol{r}}^0_m \end{bmatrix}_t + \left(\lambda^r \begin{bmatrix} \boldsymbol{A}^0 & \boldsymbol{0} \\ \boldsymbol{0}^t & \boldsymbol{0} \end{bmatrix} + \begin{bmatrix} \boldsymbol{K}^0_{bb} + \sigma_x \boldsymbol{K}^0_g & \boldsymbol{0} \\ \boldsymbol{0}^t & \boldsymbol{K}^0_{mm} \end{bmatrix} + 2 \begin{bmatrix} \boldsymbol{K}^0_{1bb} & \boldsymbol{K}^0_{1bm} \\ \boldsymbol{K}^0_{1mb} & \boldsymbol{0} \end{bmatrix} + 3 \begin{bmatrix} \boldsymbol{K}^0_{2bb} & \boldsymbol{0} \\ \boldsymbol{0}^t & \boldsymbol{0} \end{bmatrix} \right) \begin{bmatrix} \boldsymbol{r}^0_b \\ \boldsymbol{r}^0_m \end{bmatrix}_t = \begin{pmatrix} \boldsymbol{0} \\ \boldsymbol{0} \end{pmatrix} \tag{12}$$

Under these assumptions, the aeroelastic stability boundaries [in the case of a simply supported square panel (Fig. 2)] governed by the compressive load σ_x and dynamic pressure λ^r parameters are directly related to the nature of the static solutions of Eq. (11) (which can be easily solved using a Newton–Raphson algorithm), that is, in region I of the flat stable panel configuration, Eq. (11) has a converged trivial solution, in region III of the buckled stable panel configuration, a converged nontrivial solution occurs, and in region IV, bifurcation occurs and Eq. (11) fails to yield a converged real solution. Region IV is the domain of the chaotic phenomenon.

Transient Hypersonic Flow Effects

The high-speed flow effects consist of dynamic pressure and kinetic heating acting on panel substructures of hypersonic vehicles.

The thermal buckling load arises when the kinetic heating of the panel surface yields a temperature difference between the fixed edges (completely restrained against in-plane motions) and their supports. The in-plane stress resultants are equal:

$$N_x = N_y = -\frac{Eh\alpha\Delta T(t)}{1-\nu} \tag{13}$$

and could be related to the critical buckling conditions $\Delta T_{\rm cr}$ by the relation

$$-\sigma_x(t)\big|\ 2\pi^2 = \Delta T(t)/\Delta T_{\rm cr} \tag{14}$$

The phenomenon of kinetic heating modeled by standard compressible flow and shock relations confirmed[19] the pattern of a transitory temperature distribution over the panel surface until a stagnation level is reached. Under these circumstances, the same pattern can be assumed for the temperature difference ΔT, as well as for the thermal buckling load parameter σ_x.

In accord with Dowell's notations, the nondimensional dynamic pressure parameter can be expressed in relation to the Mach number and the structural and flight characteristics:

$$\lambda^r = \frac{\rho_\infty U^2_\infty a^3}{M_\infty D} = kM_\infty \tag{15}$$

where k is a coefficient depending on the panel geometry and material properties (Young's modulus and length/thickness ratio), as

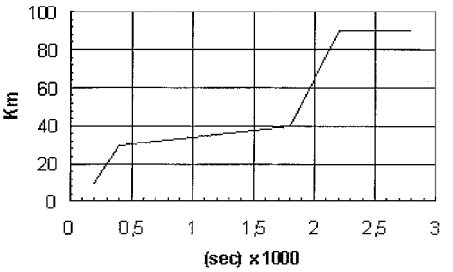

Fig. 3 Typical trajectory of a hypersonic vehicle.

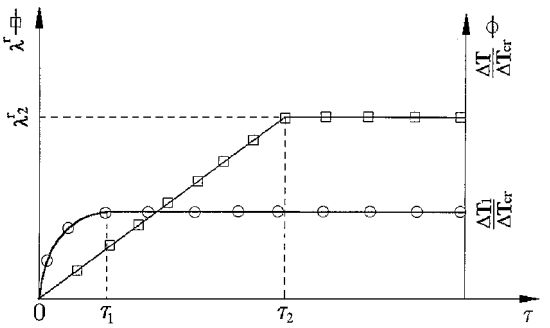

Fig. 4 Functions of parameter changes.

well as on the characteristics of the height of flight (air density and speed of sound):

$$k = \rho_\infty c^2 \frac{12(1-\nu^2)}{(h/a)^3 E} \tag{16}$$

A typical trajectory of a hypersonic vehicle (skewed in Fig. 3) also involves a transitory pattern including constant levels that can be extrapolated to dynamic pressure parameter λ^r.

By taking these considerations into account, the proper functions for the transient behavior of the parameters that govern the aerothermoelastic stability (thermal buckling load and dynamic pressures) should have increasing slopes until the steady-state (stagnation) values are reached. These assumed functions (shown in Fig. 4) are implemented into the computational program that solves the general equation (8). The nonlinear aerothermoelastic model does not have constant parameters (as does the classical approach); they vary with the transitory pattern mentioned earlier.

Results

To perform a reliable analysis, the computational program has been tested on the classical panel flutter problem: the complete behavior of a simply supported square panel ($a/b = 1$ and $h/a = 0.01$) under uniform temperature change ΔT. The nondimensional damping parameter $\delta/M_\infty = 0.01$, the static pressure $\boldsymbol{P}_s = 0$, and the in-plane dynamics were neglected ($\boldsymbol{M}^0_{mm} = 0$) in the general aeroelastic Eq. (8).

The nonlinear structural effect consists of the in-plane stretching stresses induced by the large amplitudes of the out-of-plane motion. Because the tension increases at higher and higher deflections and remains positive for any sign of the amplitude, a limited aeroelastic response [limit-cycle flutter (Fig. 5)] arises at supercritical dynamic pressures. As the map of the aerothermoelastic boundaries shows (Fig. 2), the dynamic behavior becomes more complex under certain combinations of dynamic pressures and thermal buckling loads: The limit-cycle oscillation (LCO) domain is extended at large-temperature change ($\Delta T > \Delta T_{\rm cr}$), and chaotic motions arise for moderate temperature and dynamic pressure conditions. The chaotic motion that occurs (Fig. 6) might well be termed random. However, it is clear that such motion evolves continuously in parameter space from motion that is decidedly deterministic.

The static thermoaerodynamic deflections may take place at small dynamic pressures, but at large in-plane thermal buckling loads (third region in Fig. 2). For small aerodynamic forces, the supercritical buckling forces ($-\sigma_x/2\pi^2 = \Delta T/\Delta T_{\rm cr} > 1$) will determine

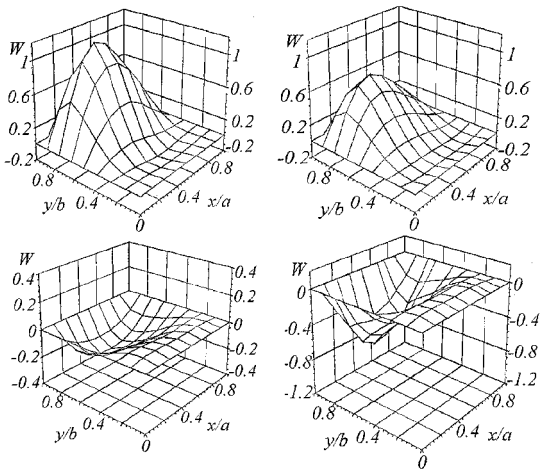

Fig. 5 LCO of the panel ($\lambda^r = 800, \sigma_x/2\pi = 0$).

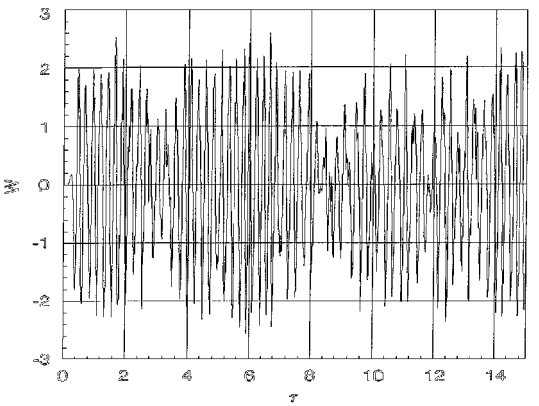

Fig. 6 Chaotic motion ($\lambda^r = 350, -\sigma^x/2\pi^2 = 3.2$) midpoint of the panel.

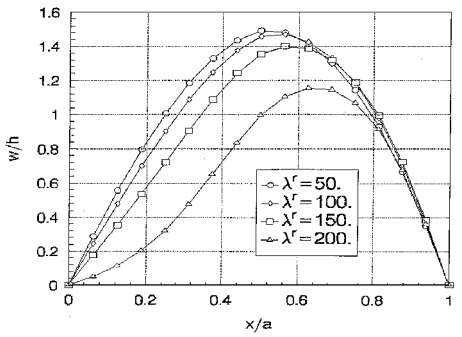

Fig. 7 Aerothermodynamic deflection at various dynamic pressures ($-\sigma_x/2\pi^2 = \Delta T/\Delta T_{cr} = 3$).

a large (almost) symmetrical thermal deflection of a simply supported panel. For increasing aerodynamic forces, the divergence shape of the panel becomes nonsymmetrical (with the maximum amplitude point tending to the trailing edge) and decreases in amplitude (Fig. 7).

The limit-cycle deformed shapes at various flow and thermal conditions can offer a better understanding of the phenomenon within the classical approach. Thus, we can see (Fig. 8) that the LCO amplitude increases when exposing the panel to higher level of thermal buckling loads under the same dynamic pressure.

The enhanced analysis performed for the transitory input data is exemplified with dynamic response diagrams (Figs. 9–16) obtained by step by step integration of the general equation system (starting from a perturbation panel deflection due to an uniform pressure distribution acting on panel surface). These nondimensional diagrams (amplitude scaled at panel thickness and dimensionless time) have the advantages of establishing scaling laws to extrapo-

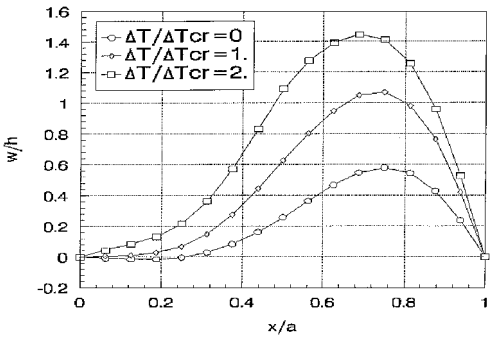

Fig. 8 Limit-cycle deformed shapes ($y = a/2$ section), various thermal conditions at $\lambda^r = 600$.

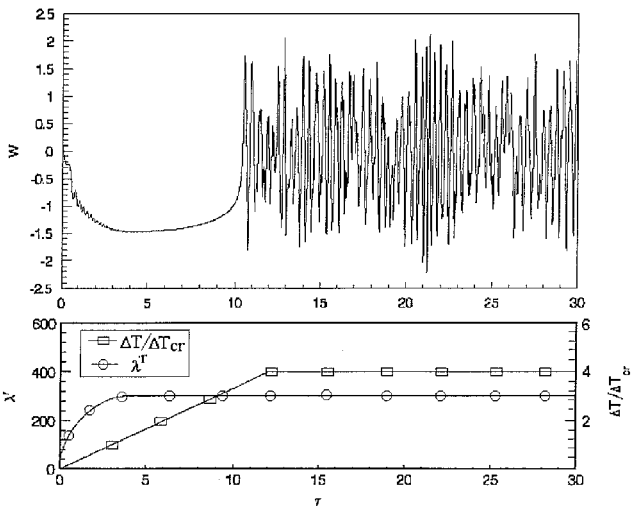

Fig. 9 Transient behavior at $\Delta T/\Delta T_{cr} \rightarrow 3$, $\lambda^r \rightarrow 400$.

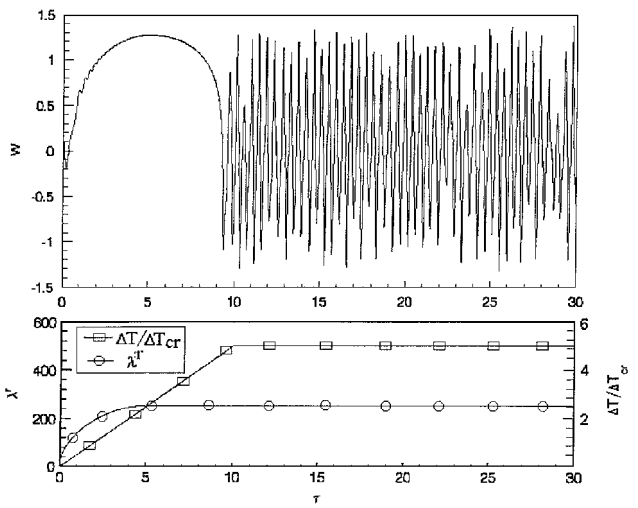

Fig. 10 Transient behavior at $\Delta T/\Delta T_{cr} \rightarrow 2.5$, $\lambda^r \rightarrow 500$.

late results for other physical situations. Each graphic (Figs. 9–16) shows the dynamic response (top) of the middle point of the panel together with the corresponding variation of the nondimensional velocity and thermal parameter (bottom, each scaled on the same diagram) that govern the motion. The geometric configuration of the structural system corresponds to an isotropic square panel having thickness/length ratio $h/a = 0.005$.

Apparently, the dynamic pattern should be related to the map of the aeroelastic stability boundaries (Fig. 2), but detailed numerical investigations do not always confirm this assumption. Figures 9 and 10 exemplify two cases of transition to certain pairs values ($\Delta T/\Delta T_{cr}$ and λ^r) when the dynamic behavior changes from a

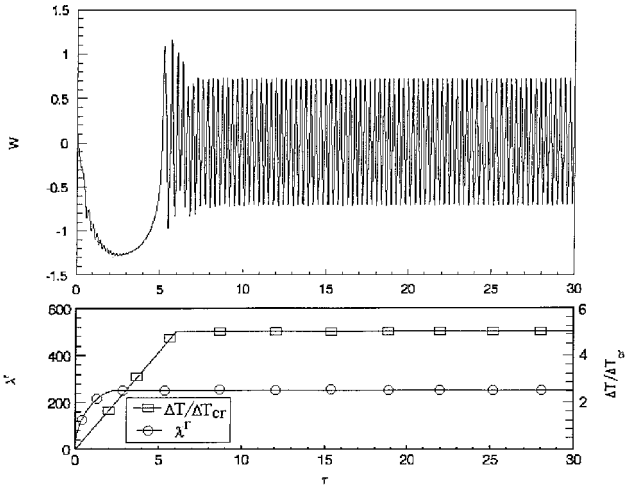

Fig. 11 Transient behavior ($\Delta T/\Delta T_{cr} \rightarrow 2.5$, $\lambda^r \rightarrow 500$) during a rapid change in dynamic pressure.

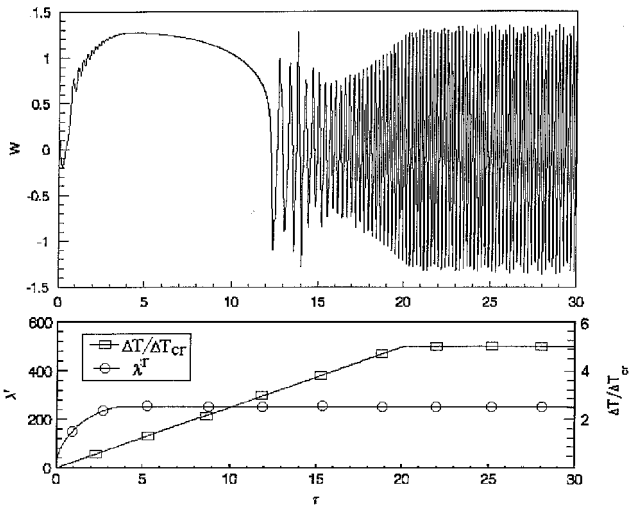

Fig. 12 Transient behavior ($\Delta T/\Delta T_{cr} \rightarrow 2.5$, $\lambda^r \rightarrow 500$) during a moderate change in dynamic pressure.

buckled panel to a chaotic pattern, though the aeroelastic stability map indicates limit-cycle flutter solutions at this value. Moreover, even when changing only the slope of the dynamic pressure function in transition to the same steady value ($\lambda^r = 500$) and under the same thermal condition (transient heating to $\Delta T/\Delta T_{cr} = 2.5$), the dynamic responses change their steady-state amplitudes and patterns (Fig. 11 buckled → limit-cycle flutter and Fig. 12 buckled → chaos → limit-cycle flutter, see also Fig. 10 for comparison). This behavior is not evinced by the aerothermoelastic stability map, which simply shows that every point of the LCO domain is uniquely characterized by a value of limit-cycle amplitude. Numerically there also can be found conditions for transition to a buckled shape of the panel that is dynamically stable under the same stagnation dynamic pressure and thermal levels. Indeed, Fig. 13 shows this, but the case is not associated with the third region of the stability map (Fig. 2) that corresponds to other combinations of parameters. This unpredictable behavior cannot be fully explained through the theory of chaotic motions in deterministic systems because the unpredictability in dynamics of chaos is usually caused by small changes in initial conditions. The dynamic responses presented here have been obtained by numerical integration starting from the same initial conditions and modifying only the rate of change in the governing parameters. These conditions may cause the system to snap to a nonzero equilibrium position (as in Fig. 13) or to oscillate with different amplitudes around the position of the flat panel (as in Figs. 10–12). This is similar to a snap-through phenomenon that is already known in thermally buckled panels. The behavior shown in Fig. 13 is less likely to appear under real circumstances because transient kinetic heating usually takes place in a very short time compared to the

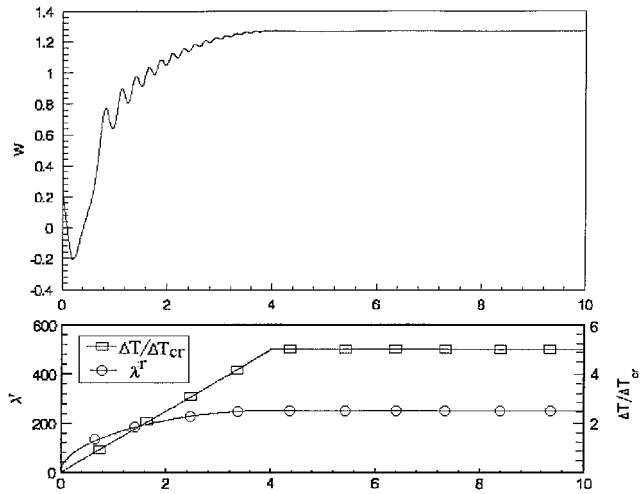

Fig. 13 Transient behavior ($\Delta T/\Delta T_{cr} \rightarrow 2.5$, $\lambda^r \rightarrow 500$) of a buckled, stable state of the panel.

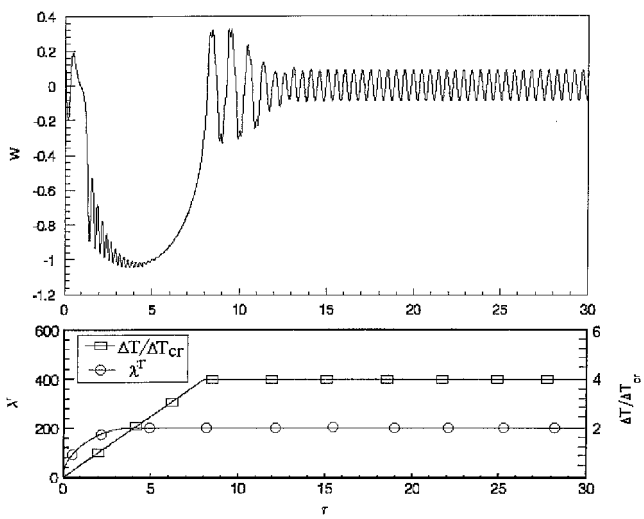

Fig. 14 Transient behavior at $\Delta T/\Delta T_{cr} \rightarrow 2, \lambda^r \rightarrow 400$ (rapid changes of governing parameters).

dynamic pressure change, and a realistic analysis should take into account this observation.

The effect of a significant difference between the transitory periods of the two parameters that govern the aeroelastic stability also consists of increasing LCO amplitude at a higher frequency. This is more evident in the two cases of transition to the same stagnation values $\Delta T/\Delta T_{cr} \rightarrow 2.5$ and $\lambda^r \rightarrow 400$ (Figs. 14 and 15 for rapid and moderate change in dynamic pressure, respectively).

Note that these are dimensionless results, and a rigorous analysis should take into account the real conditions of the phenomenon. That is why we considered it necessary to extract some dimensional values from the Dowell's parameters (9) that correspond to certain flight conditions. The case of an aluminum alloy square panel ($E = 0.735 \times 10^{11}$ Pa and $\rho_{Al} = 2767.42$ kg/m^3) is studied for three thickness/length ratios ($h/a = 0.004$, 0.005, and 0.01). Thus, the scaling relations between real and dimensionless time (τ and t, respectively) become (in seconds)

$$t = \begin{cases} 0.1603\tau, & h/a = 0.004 \\ 0.1285\tau, & h/a = 0.005 \\ 0.0641\tau, & h/a = 0.01 \end{cases} \tag{17}$$

Regarding the nondimensional dynamic pressure, a transitory behavior is equivalent to an acceleration (or deceleration) of the hypersonic vehicle at different altitudes. Table 1 gives the values of coefficient k [Eq. (16)] that relate the parameter λ^r to Mach number [Eq. (15)] depending on the altitude and panel thickness/length ratio.

Table 1 Values of coefficient k, Eq. (16)

	k		
H, km	h/a = 0.004	h/a = 0.005	h/a = 0.01
8	115.87	59.32	7.41
10	86.12	44.09	5.51
12	63.04	32.27	4.03
14	44.79	22.93	2.87
16	33.33	17.06	2.13
18	23.95	12.26	1.53
20	17.70	9.06	1.13
22	12.50	6.40	0.80
24	8.33	4.26	0.53
26	6.25	3.20	0.40
30	3.12	1.60	0.20
35	1.04	0.53	0.066
40	0.79	0.40	0.050
45	0.38	0.19	0.024
50	0.20	0.10	0.013
60	0.06	0.03	0.004
70	0.02	0.003	0.001
80	0.33×10^{-3}	1.69×10^{-3}	2.11×10^{-4}
90	5.23×10^{-4}	2.67×10^{-4}	3.35×10^{-5}

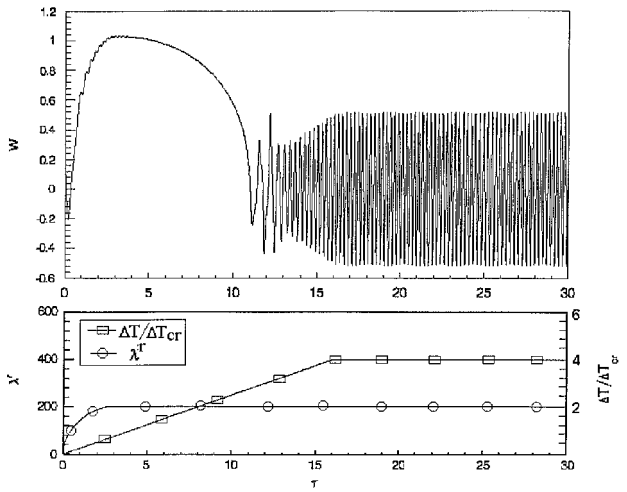

Fig. 15 Transient behavior at $\Delta T/\Delta T_{cr} \rightarrow 2$, $\lambda^r \rightarrow 400$ (moderate change of dynamic pressure).

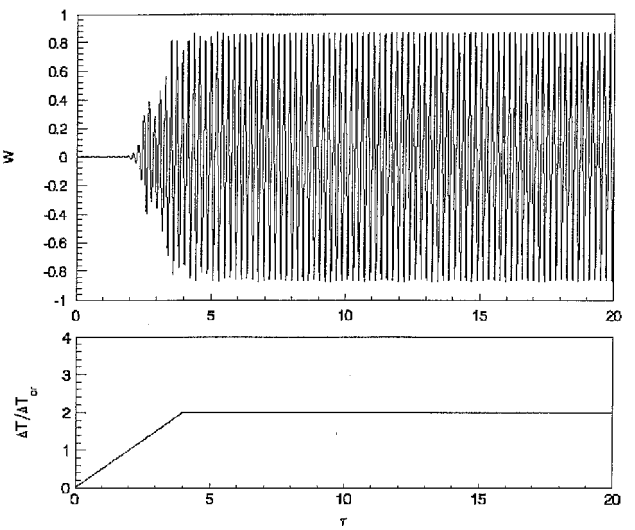

Fig. 16 Transient behavior at $\Delta T/\Delta T_{cr} \rightarrow 2$, $\lambda^r = 400$ (constant parameter).

These data are useful to define the transition period of the dynamic pressure knowing the changes in speed (Mach number) and altitude over a time span (skewed in Fig. 3). Considering the possible flight regimes of the actual high-speed vehicles, we can conclude that this phenomenon usually involves small to moderate values of dynamic pressures and could take a long time (hundreds of seconds until a stagnation value arises) compared to the transient kinetic heating.

Assuming quasi-steady conditions for the dynamic pressure during a transient behavior of thermal buckling loads, the aerothermoelastic response is also distinct from the earlier patterns. Thus, in the case of transitory thermal change $\Delta T/\Delta T_{cr} \rightarrow 2$ at $\lambda^r = 400$ [quasi-state dynamic pressure (Fig. 16)] the LCO pattern is maintained, but at larger amplitude than the cases of Figs. 14 and 15. Additional numerical investigations of this case confirmed the invariance of the LCO characteristics when varying the slope of the transitory thermal function. For this case of transitory conditions, the sensitivity of the aerothermoelastic system in LCO amplitude and frequency seems to be governed by the dynamic pressure because it is associated with the transitory change of this parameter.

Conclusions

Under fully transitory hypersonic flow conditions (simultaneous changes in thermal forces and dynamic pressures), the dynamic analysis of the panel substructures of high-speed vehicles demonstrates the complexity of the aerothermoelastic behavior. Depending on the rate of change in dynamic pressures and thermal loads, the dynamic response modifies its pattern when crossing the stable/unstable domains of a stability map. Apparently, the dynamic pattern should be related to this classical map, but detailed numerical investigations do not always confirm this assumption. The sensitivity of the nonlinear aerothermoelastic model to initial conditions and energy received by the system from the transitory governing parameters (which is characteristic of chaotic systems) could explain this complex behavior.

The classical approach of the failure prediction in panel flutter (based on the curves of constant amplitudes plotted on the area of the LCOs domain) could offer incomplete or erroneous information. A reliable fatigue and failure analysis should take into account the transient effects of hypersonic flow conditions on aerothermoelastic behavior.

Acknowledgments

This work has been supported by a grant from the Italian Consiglio Nazionale delle Ricerche under the NATO Fellowship Program. R. Udrescu wishes to thank the Department of Aeronautical and Space Engineering of the Politecnico di Torino for the computer facilities and for help in preparing this manuscript.

References

[1] Moon, F. C., *Chaotic Vibrations—An Introduction for Applied Scientists and Engineers*, Wiley, New York, 1987, pp. 7–10.

[2] Dowell, E. H., "Nonlinear Oscillations of a Fluttering Plate II," *AIAA Journal*, Vol. 5, No. 10, 1967, pp. 1856–1862.

[3] Dowell, E. H., "Nonlinear Oscillations of a Fluttering Plate," *AIAA Journal*, Vol. 4, No. 7, 1966, pp. 1267–1275.

[4] Dowell, E. H., "Panel Flutter: A Review of the Aeroelastic Siability of Plates and Shells," *AIAA Journal*, Vol. 8, No. 3, 1970, pp. 385–399.

[5] Olson, M. D., "Some Flutter Solutions Using Finite Elements," *AIAA Journal*, Vol. 8, No. 4, 1970, pp. 747–752.

[6] Han, A. D., and Yang, T. Y., "Nonlinear Panel Flutter Using High-Order Triangular Finite Elements," *AIAA Journal*, Vol. 21, No. 10, 1983, pp. 1453–1461.

[7] Xue, D. Y., and Mei, C., "Finite Element Nonlinear Panel Flutter with Arbitrary Temperatures in Supersonic Flow," *AIAA Journal*, Vol. 31, No. 1, 1993, pp. 154–162.

[8] Dixon, R. I., and Mei, C., "Finite Element Analysis of Large-Amplitude Panel Flutter of Thin Laminates," *AIAA Journal*, Vol. 31, No. 4, 1993, pp. 701–707.

[9] Zhou, R. C., Xue, Y., and Mei, C., "Finite Element Time Domain: Modal Formulation for Nonlinear Flutter of Composite Panels," *AIAA Journal*, Vol. 32, No. 10, 1994, pp. 2044–2052.

[10]Lai, Z., Xue, D., Huang, J.-K., and Mei, C., "Panel Flutter Limit-Cycle Suppression with Piezoelectric Actuation," *Journal of Intelligent Material Systems and Structures*, Vol. 6, No. 3, 1995, pp. 274–282.

[11]Zhou, R. C., Lai, Z., Xue, D., Huang, J.-K., and Mei, C., "Suppression of Nonlinear Panel Flutter with Piezoelectric Acuators Using Finite Element Method," *AIAA Journal*, Vol. 33, No. 6, 1995, pp. 1098–1105.

[12]Zhou, R. C., Mei, C., and Huang, J.-K., "Suppression of Nonlinear Panel Flutter at Supersonic Speeds and Elevated Temperatures," *AIAA Journal*, Vol. 34, No. 2, 1996, pp. 347–354.

[13]Xue, D. Y., and Mei, C., "Finite Element Nonlinear Flutter and Fatigue Life of Two-Dimensional Panels with Temperature Effects," *Journal of Aircraft*, Vol. 30, No. 6, 1993, pp. 993–1001.

[14]Udrescu, R., "Failure Prediction of the Fluttering Panels in Supersonic Flow," *Proceedings of the 27th Scientific Session of the Romanian Academy of Military Technique*, Bucharest, Romania, 1997, pp. 193–200.

[15]Udrescu, R., "A Higher Finite Element Model in Nonlinear Panel Flutter Analysis," *Proceedings of the AIAA/ASME/ASCE/AHS/ACS 39th Structures, Structural Dynamics, and Materials Conference*, AIAA, Reston, VA, 1998, pp. 1252–1262.

[16]Udrescu, R., "Aero-Thermoelastic Behaviour of Panel Substructures Subjected to Rapid Accelerations in Supersonic Flow," *7th AIAA/USAF/NASA/ISSMO Symposium on Multidisciplinary Analysis and Optimization*, pp. 1011–1018.

[17]Bailie, J. A., and McFeely, J. E., "Panel Flutter in Hypersonic Flow," *AIAA Journal*, Vol. 6, No. 2, 1968, pp. 332–337.

[18]Argyris, J., and Mlejnek, H. P., *Die Metoden der Finiten Elementen*, Vols. 1–3, Vieweg, Braumschweig, Germany, 1986–1988, pp. 742–762.

[19]Kontinos, D., "Coupled Thermal Analysis Method with Application to Metallic Thermal Protection Panels," *Journal of Thermophysics and Heat Transfer*, Vol. 11, No. 2, 1997, pp. 173–181.

A. N. Palazotto
Associate Editor